

# **Thermodynamics of the Solid-Liquid Phase Boundary of Deuterium**

Erin Wang

Brighton High School  
Rochester, NY

Advisor: Dr. David Harding

Laboratory for Laser Energetics  
University of Rochester  
Rochester, NY  
November 2013

## Abstract

Cryogenic targets used for inertial confinement fusion experiments contain a deuterium-tritium (DT) ice layer that begins to melt when the protective shroud is removed to implode the target. Heat (from ambient radiation) absorbed in the plastic shell creates a “slush” (partially melted) region at the plastic/ice interface that expands with time to encompass the entire DT fuel layer. The increasing fraction of the lower-density liquid in this slush region generates a volumetric expansion that buckles the surface of the ice layer making it less hydrodynamically stable when imploded. Little is known of the early-time response of the target to this heat load and whether this behavior is important for the brief time lapses used for current and future ICF targets (0.1 s and up to 5 s, respectively).

The experiments performed here applied a controlled heat load to deuterium ice inside a calorimetry cell and measured how the energy was partitioned between melting the ice and raising the temperature of the liquid fraction in the region. A 0.62 mg sample of deuterium ice (equivalent to a 270  $\mu\text{m}$  thick ice layer in an ignition target) at a temperature marginally below the triple point of  $\text{D}_2$  (18.733 K) was heated at different rates. It was determined that  $\sim 20$   $\mu\text{m}$  of the 270  $\mu\text{m}$  ice layer would melt with 5 seconds of exposure to a blackbody radiation load that a NIF target would see. Most (90 to 95%) of the heat was expended melting the ice; the remainder was used to raise the temperature of the liquid. These data quantify the importance of minimizing the time the target is exposed to ambient radiation.

## 1. Introduction

Inertial confinement fusion (ICF) target designs for fusion experiments are shown in Fig.1 for three different laser drivers. The targets for OMEGA and the National Ignition Facility (NIF) consist of a hard plastic shell, an inner shell of solid deuterium-tritium (DT), and a central core of DT gas. The NIF target is larger and contains more DT fuel than the OMEGA target, in proportion to the relative power of the lasers. This target is designed to achieve ignition at the NIF. The third type of target is proposed for inertial fusion energy (IFE) and adds a low-density foam layer filled with solid DT.

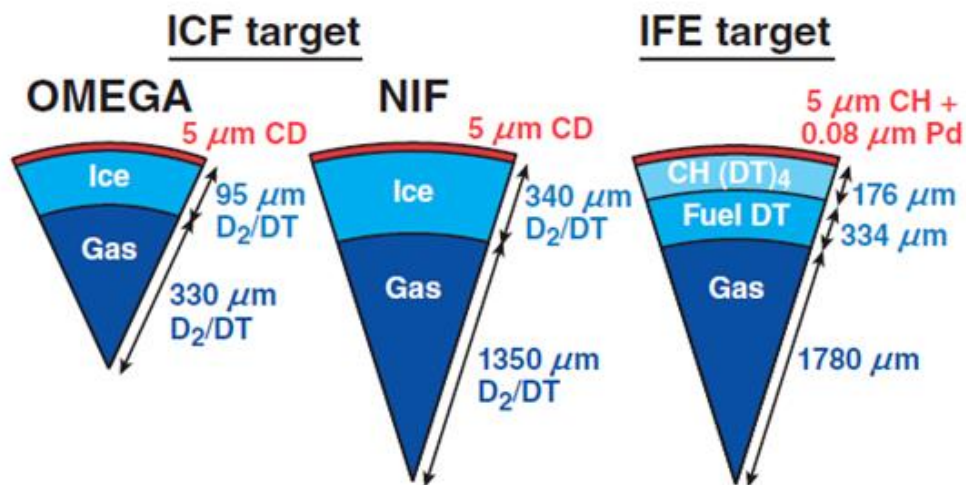


Fig. 1. Design of cryogenic targets for use at OMEGA and the NIF, and a possible future IFE target.

Cryogenic targets for OMEGA and NIF ICF experiments contain a DT ice layer that will rapidly warm up when the targets are exposed to ambient blackbody radiation before the implosion. The radiant energy is absorbed in the outer plastic capsule causing the temperature of the D<sub>2</sub> ice closest to the plastic to rise faster than the inner surface of the ice layer. (For reference, the temperature of a DT target rises at a rate of ~0.077 K/s based on the heat capacity

of the solid and volumetric heating from tritium decay, without any radiative heating, and the target fully melts in 250 s.) Once the temperature reaches the triple point value for deuterium the ice begins to melt. Importantly, over the time period that is relevant to ICF targets (0.1 s and 5 s for OMEGA and NIF targets, respectively), only the ice nearest to the plastic melts before the target is imploded.<sup>1</sup> However, because the heat that continues to be deposited in the plastic during that period will both flow to the cooler inner surface of the ice layer and also be consumed melting the ice (and raising the temperature of the liquid), it is unclear how much ice will melt.

An example of this phenomenon is shown in Fig. 2 for an IFE target that will experience a sizeable heat load during the 0.05 s it is inside a fusion reactor before it is imploded.<sup>2</sup> The lower density of the liquid (0.18 gm/cm<sup>3</sup> for liquid D<sub>2</sub> compared to 0.2 gm/cm<sup>3</sup> for the solid D<sub>2</sub> used in these experiments; DT liquid and solid used in fusion targets have proportionally higher densities) generates a volumetric expansion stress that will buckle the inner surface of the ice layer rather than the plastic (which is significantly stiffer than the ice and better resists the applied stress). The magnitude of buckling will be proportional to the extent of melting.

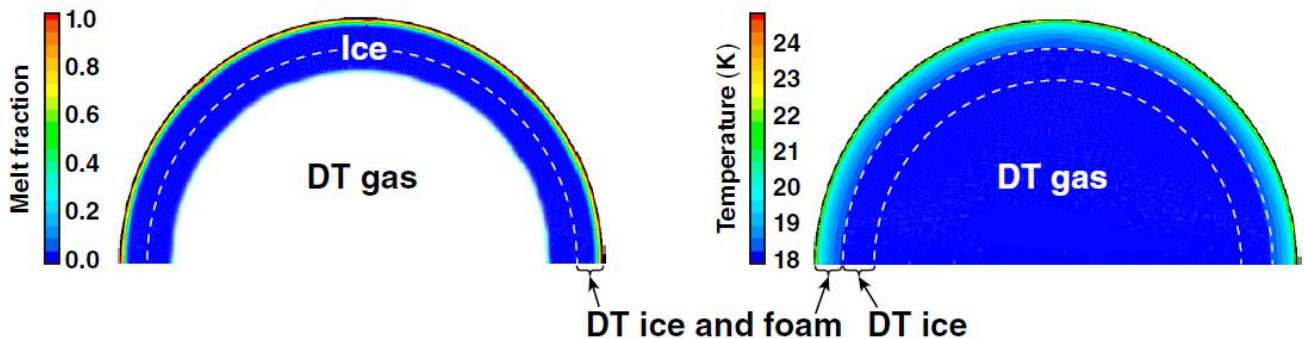


Fig. 2. The melt fraction (a) and temperature (b) of an IFE target calculated for a heat load of 50 kW/m<sup>2</sup> at the surface of the target. The diameter of the target is 4.5 mm and the thickness of the ice layer is 0.35 mm. After 0.05 s the outer portion of the ice layer has completely melted while the temperature of the inner ice surface is unchanged.

The calculated effects of ambient radiation on an OMEGA target (5- $\mu\text{m}$  plastic ablator and a 100- $\mu\text{m}$  D<sub>2</sub> ice layer)<sup>1</sup> are shown in Fig. 3. The temperature of the ice at the outer surface rose from an initial value of 17.0 K to the triple point value in 0.05 s (Fig. 3a). After 0.1 s, 2.4% of the ice closest to the plastic wall has melted. (Fig. 3b) The limitation with this calculation is the uncertainty of how to partition the available energy between melting the ice and flowing to the internal surface of the ice layer where it sublimates the ice.

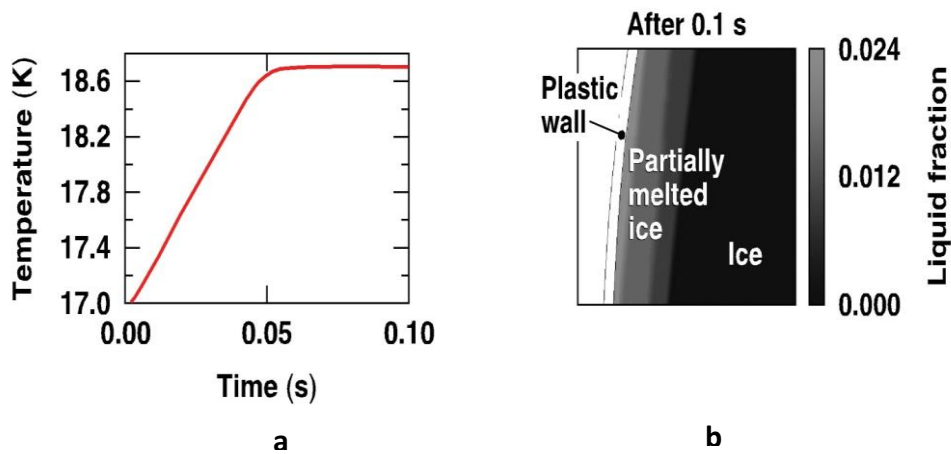


Figure 3. (a) Time-dependent temperature of the outer surface of the ice layer and the (b) liquid fraction in the ice layer after 0.1 s.

The roughness of the target's DT ice surface is measured prior to retracting the protective shroud, but not after the shroud is retracted: no diagnostic is available that can evaluate the target's roughness with sufficient resolution at the center of a 6-m diameter vacuum chamber in the brief time before it is exploded. The roughness that develops in that intervening period will create hydrodynamic instabilities that cause the target to break up and reduce the pressure in the hot spot. That roughness value needs to be inferred from experiments that can separately

quantify each of the possible causes for roughness. The data obtained here are a necessary first step to implement accurate experimental corrections to improve target uniformity.

## **2. Experimental Methods**

### **2.1. The calorimetry cell**

The goal of this experiment was to demonstrate that a calorimetry cell containing an amount of  $D_2$  comparable to that found in an ICF target could be used to measure how rapidly the  $D_2$  ice responded when heated above the melting temperature. A calorimetry cell works by applying a known amount of heat to a thermally isolated system and measuring the resulting change in temperature. The rate at which the temperature of an empty cell changes with time is determined by the heat capacity of the materials (which is well known) and the amount of heat applied. Adding  $D_2$  to the cell slows the rate at which the temperature changes as additional heat is needed to compensate for the heat capacity ( $C_p$ ) of  $D_2$ . That rate slows further when the temperature reaches the ice's freezing temperature (18.73 K; heat of fusion is 199 J/mol). The feasibility of this concept was demonstrated in earlier experiments where the calorimetry cell had a heater and temperature sensor connected directly to the cell.<sup>3</sup> However, that design lacked the ability to provide small heat loads needed to replicate the heating of a target and the sensitivity needed to measure small differences in the rate of temperature rise between a  $D_2$ -filled and empty cell when a small quantity of  $D_2$  (such as the amount present in an ICF target) was used.

The earlier calorimetry cell was redesigned for these experiments to be smaller (to lower the  $C_p$  of the cell) and to better control the small amount of heat that needed to be applied; heaters that are large enough to balance the multi-watt cooling power of the cold head lack the

precision to provide sub-milli-watt level control of the output; and applying too much heat will melt the ice too rapidly to diagnose the melting process.

Images of the cell are shown in Fig. 4 and the design concept is shown in Fig. 5. The cell consisted of a copper cube (1.22 cm<sup>3</sup> volume; weighing 24.87 gm) with a cylindrical hole through the vertical axis. Sapphire windows (3.2 gm) on the top and bottom of the cell were attached to the copper cell with steel flanges (3.68 gm) to form a vacuum-tight seal. The cell was connected by a thin wire (10 cm x 1.6 mm diameter) to a copper mass that functioned as a thermal reservoir. D<sub>2</sub> gas was added to the cell through a thin-wall narrow diameter steel tube that was connected to a gas manifold. The steel tube was attached (via a copper wire) to the first stage of a cold head (35 K) to intercept heat flowing from the gas manifold (at room temperature) to the cell.

A heater connected to the reservoir controlled the temperature of the entire system; heat flowed from the cell to the reservoir down the single copper wire. The reservoir was connected to a cold head (CryoMech), which was maintained at 12 K and functioned as a heat sink for the calorimetry cell. One temperature sensor was attached to the cell and a second sensor was attached to the reservoir. The sensor was sensitive enough to detect 0.001 K changes in temperature. A test of the sensitivity of the cell to small temperature changes was to switch the room lights off, which (Fig. 6) registered a 0.001 K decrease in temperature, followed by a 0.001 K increase when the light were switched on. A more extreme test was to switch on a blue LED beneath the cell (set to 4 V), as a result of which the calorimetry cell recorded a 0.005 K change in temperature.

The entire cell was contained within a vacuum-sealed copper radiation shield and the viewing windows were insulated with 3-mm thick gold-coated infrared radiation absorbent glass.

The calorimetry cell was sufficiently isolated from ambient radiation that it could detect heat changes as small as 0.0002 J.

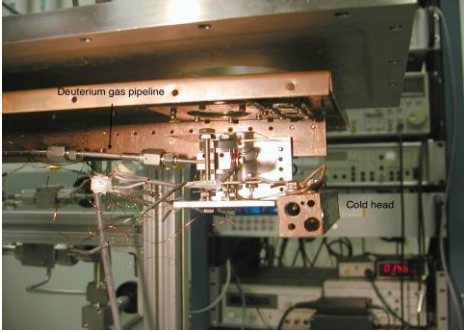


Fig. 4a. Side view of calorimetry cell. Deuterium is fed through a pipeline into the cell. The thermal reservoir is visible in this photo.

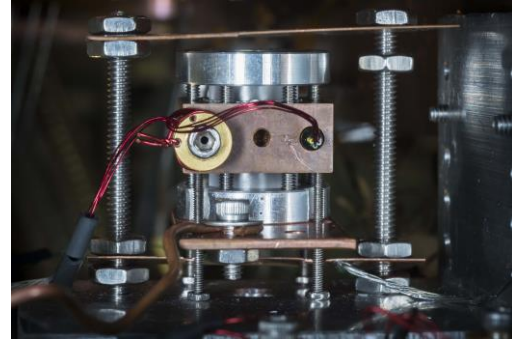


Fig. 4b. Front view of calorimetry cell. Deuterium contained within the chamber is heated by a wire running between the cell and heat reservoir.

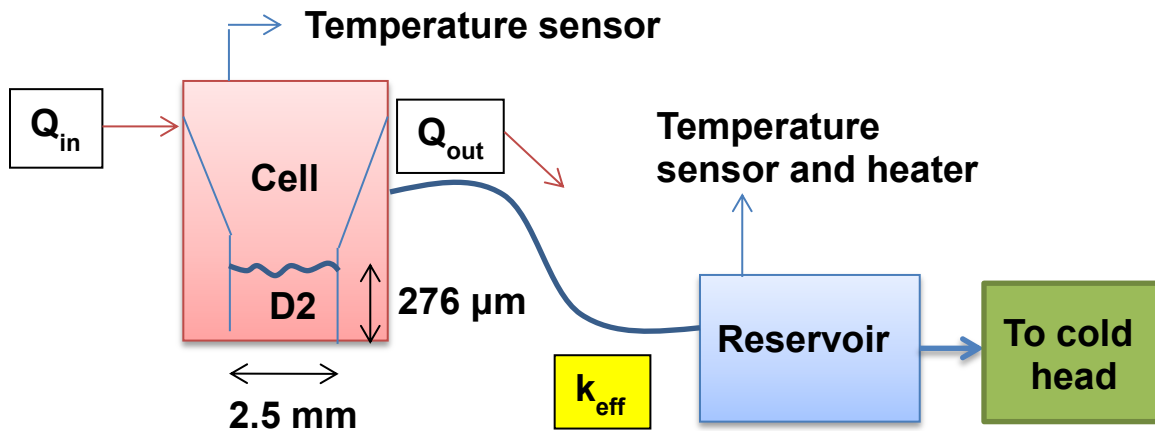


Fig. 5. Schematic diagram of calorimetry cell. Temperature sensors located in the cell and reservoir measure changes in temperature that allow the thermal conductivity ( $k$ ) of the wire connecting the cell and reservoir to be calculated.  $Q_{in}$  represents the heat load into the cell from radiation and thermal conduction sources and, in steady state, balances the heat load  $Q_{out}$  conducted, through the wire, out of the cell.

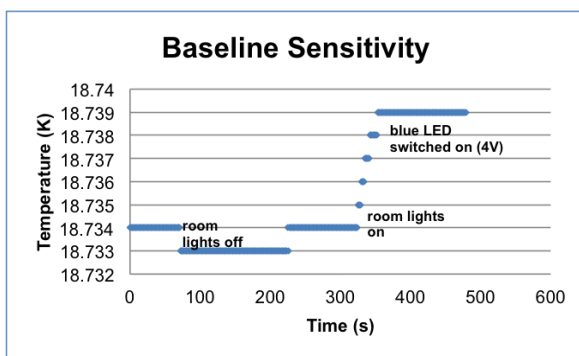


Fig. 6. The sensitivity of the calorimetry cell is demonstrated by switching the room lights on and off to produce a 0.001 K temperature change. Activating the blue LED that can be used to view the ice layer (but was not done in these experiments) increased the temperature by 0.005 K.

When the cell temperature was  $\sim 19$  K the valve separating the gas manifold and cell was opened and a controlled amount of  $D_2$  condensed inside the cell. The deuterium formed a 2.5-mm diameter and  $\sim 270$ - $\mu\text{m}$  high cylinder at the bottom of the cell. The base of the  $D_2$  liquid cylinder contacted the sapphire window and the vertical sides contacted the copper cell. Importantly, copper and sapphire are both very thermally conductive ensuring that the cell and  $D_2$  were isothermal to within 0.001 K. Heating the cell caused the outer surface of the  $D_2$  cylinder contacting the copper and sapphire to heat first and the internal volume of the  $D_2$  heated more slowly. In this way the cell approximates a target with the difference that the  $D_2$  shape is cylindrical rather than spherical.

## 2.2. Experimental process

For each experiment the temperature of the cell was initially below the triple point temperature of  $D_2$  ( $\sim 18.73$  K, the unique temperature where the liquid, solid and vapor phases co-exist). At steady state conditions the temperature of the reservoir was  $\sim 0.4$  K lower than the

temperature of the cell, and the heat load into the cell from radiation and thermal conduction sources ( $Q_{in}$ , Watts) equaled the heat load out of the cell to the reservoir ( $Q_{out}$ ). (Fig. 5)

Heat was added to the cell by raising the temperature of the reservoir by a controlled amount (0.02, 0.05, 0.1 and 0.3 K) using the heater attached to the reservoir. The time required for the reservoir to reach the higher temperature value ranged from <1 to 7 s, depending upon the size of the temperature step. It is important to note that increasing the temperature of the reservoir did not cause heat to flow from the reservoir to the cell; the reservoir temperature was lower than the temperature of the cell all times. Heat flowing into the cell ( $Q_{in}$ ) from external sources remained constant at all times while heat flowing out of the cell to the reservoir ( $Q_{out}$ ) decreased temporarily as the temperature gradient between the cell and reservoir decreased. During that period the additional heat flow  $\Delta Q$  into the cell ( $\Delta Q = Q_{in} - Q_{out}$ , which increased as  $Q_{out}$  decreased) raised the cell temperature, which raised the temperature gradient and caused  $Q_{out}$  to rise and  $\Delta Q$  to decrease. Ultimately, a higher and stable cell temperature was achieved and the temperature gradient between the cell and reservoir returned to the original value. The time required for the cell to converge to this new higher temperature ranged from 20 to 50 s and depended upon the net heat load available to the cell ( $\Delta Q$ ) and the heat capacity of the cell.

The rate of change of  $Q_{out}$  determined the duration and amount of surplus energy available to heat the cell and depended on the physical dimensions and thermal conductivity of the thin copper wire (as well as the thermal resistance of the connections between the copper wire and the cell and reservoir), and the temperatures of the cell and reservoir. Previous experiments tested different lengths and thicknesses of the copper wire to provide a suitably weak thermal link between the cell and reservoir that was strong enough to cool the cell from room temperature to 18.7 K in a reasonable duration (8 h), and weak enough that the time

required for the temperature of the cell to re-establish a steady-state value would be longer than that of the reservoir ( $> 20$  s and  $< 3$  s, respectively).<sup>3</sup>

The first step towards calculating the amount of heat flowing into the cell was to calculate the thermal conductivity of the copper wire connecting the cell and reservoir; D<sub>2</sub> was not present in the cell for these experiments. The temperature of the reservoir was raised by 0.02 K. The temperatures of the cell and reservoir were recorded every second and the temperature difference ( $\Delta T_i$ ) for each time step (i) of duration  $\Delta t$  was calculated for the duration of the temperature transient until thermal equilibrium was re-established. The corresponding heat flow out of the cell during that time step,  $q_{out,i}$  depends on the temperature difference and the thermal conductivity ( $k$ ) of the wire (which is constant) according to Fourier's Law.

$$q_{out,i} = k * \frac{A}{l} * \Delta T_i \quad (1)$$

where  $A$  and  $l$  are the cross-sectional area and length of the wire, respectively.

The resulting heat flow available ( $q_i^{available}$ ) to raise the temperature of the cell varied with time:

$$q_i^{available} = Q_{in} - q_{out,i} \quad (2)$$

where  $Q_{in}$ , which does not change during the experiment, is given by Fourier's law under steady-state conditions.

$$Q_{in} = k * \frac{A}{l} * (T_{cell}^{steady-state} - T_{reservoir}^{steady-state}) \quad (3)$$

The total amount of energy needed to raise the temperature of the cell, equal to the product of the heat capacity of the cell ( $C_p = 0.198$  J/K) and the change in temperature of the cell ( $\Delta T = T_{cell, final} - T_{cell, initial}$ ), was equated to the total available energy:

$$C_p \cdot \Delta T = \sum_i^N q_i^{available} \cdot \Delta t \quad (4)$$

where N is the number of time steps during the temperature transient. The thermal conductivity was calculated from equations (1) - (4).

The calculation was repeated using the  $\Delta T$  values measured for each of three temperature step changes to the reservoir (0.05, 0.1 and 0.3 K, and a repeat of the 0.1 K step change). The average thermal conductivity from these five measurements was  $998 \pm 35$  W/m/K. This thermal conductivity value is realistic; it corresponds to high purity copper wire with a RRR (residual resistance ratio) of  $\sim 50$ , which suggests that the thermal resistance at the wire connections is not a large contributor to the overall thermal resistance. Using this value for  $k$ , the steady state heat load to the cell from radiative and conductive heat loads (which accounts for the cell being 0.387 K warmer than the reservoir) was 0.0083 W.

Figure 7 shows the measured time-dependent response of the temperature of the cell (solid red line) and the reservoir (black dotted line) when the temperature of the reservoir was increased from 18.332 to 18.352 K. The cell temperature calculated using the average thermal conductivity value obtained from all the experiments (the dashed blue line) agreed closely with the measured value. The temperature of the reservoir re-established a steady state value within 3 s of the initial temperature change, while the temperature of the cell required  $\sim 30$  s to stabilize.

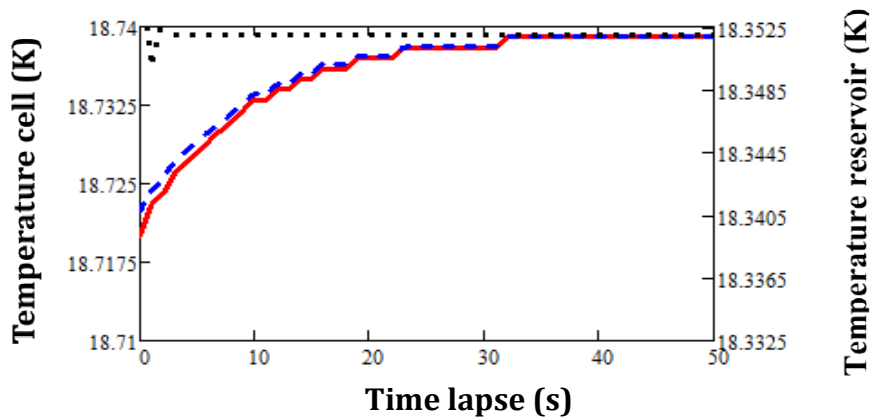


Fig. 7. Temperature profile for the cell (red solid line) and the reservoir (black dotted line) when heated by 0.02 K. The blue dashed line is the temperature of the cell calculated using the heat capacity value and the averaged thermal conductivity (derived above).

The amount of deuterium added to the cell was determined using the following protocol: D<sub>2</sub> gas was added to a calibrated volume (40 cm<sup>3</sup>) and gas manifold (12.7 cm<sup>3</sup>) that combined possessed a significantly larger volume than the cell (calculated to be 1.2 cm<sup>3</sup> from the dimensions of the components). The pressure of the gas in the calibrated volume was recorded and the gas then expanded into the cell. The amount of D<sub>2</sub> in the cell was 0.0015 gm. The volume of the cell was calculated from the change in pressure to be 1.22 cm<sup>3</sup>, in good agreement with the value calculated from the cell's dimensions. The cell was isolated from the vacuum manifold and cooled to 18.72 K to first liquefy the gas in the cylindrical base of the cell and then solidify the liquid. The steady-state vapor pressure of the gas above the ice was calculated using the D<sub>2</sub> equation of state and the amount of D<sub>2</sub> in the gas phase was determined knowing the volume of the cell. The remaining mass was in the form of ice (0.0006 gm at 18.72 K). This mass is equivalent to the amount of fuel in a NIF direct drive ignition target with a 270 μm thick

ice layer. The surface area of the ice was calculated from the known D<sub>2</sub> ice mass and the dimensions of the cylindrical bore of the cell.

### 3. Results and Discussion

The experiments described above to measure the thermal conductivity of the copper wire were repeated with solid deuterium in the cell: the temperature of the reservoir was initially set to a value where the temperature of cell was stable at 18.72 K, and the temperature of the reservoir was then increased in 0.02, 0.05 and 0.1 K steps. The temperature of both the reservoir and cell were recorded every second. The 0.02 and 0.05 K increases did not produce a sufficiently large heat flux for long enough to melt a measurable fraction of the ice. Further, the heat load and flux were calculated to be much lower than a cryogenic target will experience before it is imploded and consequently were not of interest. The effect of a 0.1 K increase in temperature was clearer; the temperature of the deuterium-filled cell rose notably slower than it did when the cell was empty (Fig. 8) once the cell temperature reached 18.734 K, and the difference became more apparent at 18.742 K. It is important to note that the temperature of the cell was not constant while the deuterium ice was melting, rather the temperature of the copper cell and liquid continued to rise together while the remaining ice melted.

The heat flowing into the D<sub>2</sub> ( $q_i^{net}$ ) at time step  $i$  was calculated from the difference in available heat flows between an empty cell and one filled with D<sub>2</sub>, ( $q_i^{net} = q_i^{D2\_filled\_cell} - q_i^{empty\_cell}$ ). This was proportional to the temperature difference between the two cases according to Fourier's Law. (Fig. 9) The energy first raised the temperature of the solid to the melting temperature, then began to melt the ice, and finally raised the temperature of the liquid while simultaneously melting the remaining ice. Given the thinness of the ice layer (<300 μm), and the

high thermal conductivity of the ice and liquid (0.38 and 0.12 W/m/K, respectively), the temperature of the liquid was assumed to be the same as the temperature of the cell, whereas the temperature of the ice remained clamped at the triple point value.

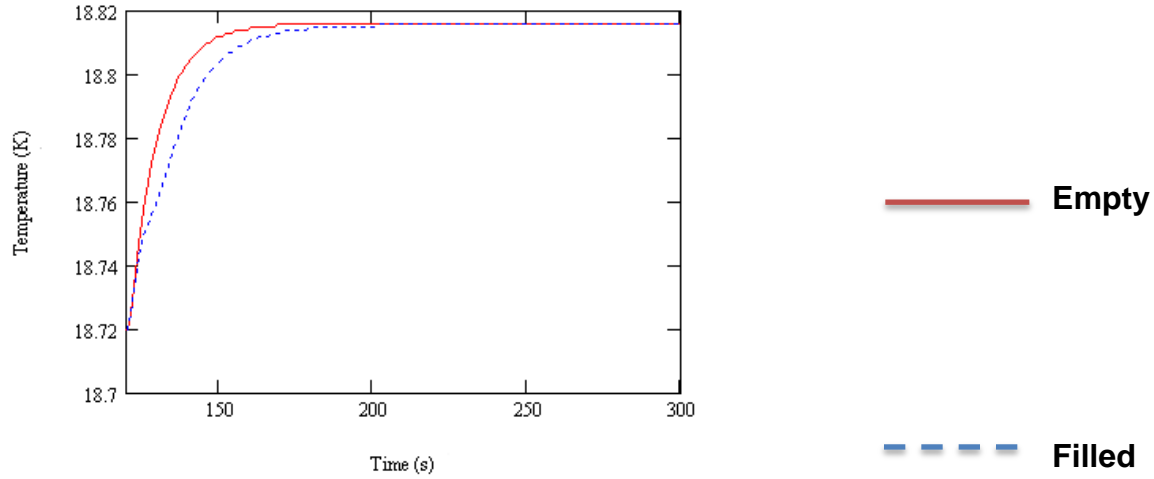


Figure 8. Temperature profiles of the cell containing D<sub>2</sub> (dotted blue line) and empty (red line) in response to a 0.1 K temperature increase.

Initially only ice was present in the cell so all the heat coupled into the D<sub>2</sub> was used to melt the ice. As liquid formed a portion of the heat was used to raise the temperature of the liquid to match the temperature of the cell. The partition of the available energy ( $q_i^{net}$ ) between melting the ice ( $q_i^{melting\_ice}$ ) and heating the liquid ( $q_i^{heating\_liquid}$ ) in each time step ( $i$ ) is defined by Eqn. 5.

$$q_i^{melting\_ice} = q_i^{net} - C_{p_{liq}} * [(T_i^{D_2-filled} - T_{i-1}^{D_2-filled})] * m_{liq} / \Delta t \quad (5)$$

where  $T_i^{D_2-filled}$  is the temperature of the D<sub>2</sub>-filled cell at time increment  $i$ ,  $C_{p_{liq}}$  is the heat capacity of liquid D<sub>2</sub> (5472 J/kg/K), and  $m_{liq}$  is the total mass of the liquid. The mass of ice that melted ( $mass_{ice\_melted,i}$ ) in each time interval was calculated knowing the heat of fusion ( $H_{fusion} = 49,500$  J/kg) from Eqn. 6.

$$mass_{ice\_melted,i} = \frac{q_i^{melting\_ice}}{H_{fusion}} * \Delta t \quad (6)$$

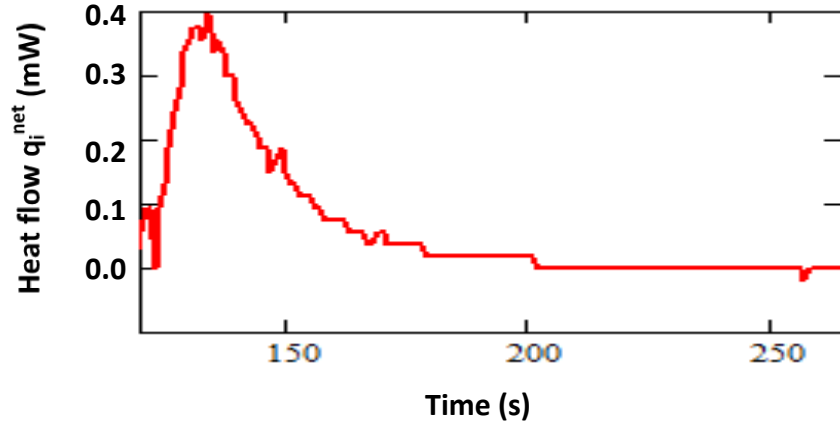


Fig. 9. The time-dependent flow of heat  $q_i^{net}$  into the cell that was available to melt the ice and heat the liquid, obtained from the temperature profiles of Fig. 8.

The greatest heat load (0.4 mW) into the D<sub>2</sub> ice occurred during the initial ~10 seconds after the temperature of the reservoir was raised by 0.10 K. The heat load plateaued for ~10 seconds and began to decrease as the temperature gradient between the cell and reservoir increased and the temperature of the cell stabilized. The decreasing heat load to the D<sub>2</sub> with time reduced the rate the ice melted: after 80 s an estimated 30% of the ice had melted and after 780 s 60% of the ice had melted. The most relevant information was obtained during the initial ~20 s when the heat load, and the corresponding heat flux (based on the surface area of the cell), were comparable to the conditions a direct drive NIF target with a reflective gold coating will experience when it is exposed to ambient radiation. The heat flux into the ice was determined by dividing  $q_i^{net}$  by the surface area of the cylinder of D<sub>2</sub> ice/liquid in contact with the cell walls. (Heat conduction through the vapor to the top surface of the ice cylinder that did not contact the

copper walls was neglected because the thermal conductivity of D<sub>2</sub> vapor is sufficiently small that heat conducted through this path will not affect the ice on the time scales studied here.) The depth and surface area of the ice/liquid were calculated from the known geometry of the cell, the amount of D<sub>2</sub> present, and the D<sub>2</sub> liquid density at 18.72 K. The heat loads into different ICF targets are displayed in Fig. 10 for comparison with the experimental values obtained for the calorimetry cell.

The fraction of heat used to melt the ice ( $\frac{q_i^{melting\_ice}}{q_i^{net}}$ ) and the resulting increase in the thickness of the liquid D<sub>2</sub> layer at each time increment are shown in Fig. 11. The liquid layer in this study is defined as consisting of only liquid, although in reality the liquid will exist in a much thicker ice/liquid “slush” layer, with the liquid fraction decreasing with increasing distance from the copper surface. (The amount of liquid present is reported as a 100% liquid layer because the experiment is unable to determine the thickness and composition of this “slush” region.) The data most relevant to an ICF target is the first ~20 s of the heating cycle when 90 to 95% of the incident heat load was used to melt the ice. From the maximum slope of the dotted blue line, ~4 μm of liquid D<sub>2</sub> is formed every second, or ~ 20 μm during a 5-s period. The conversion of a ~20-μm thick layer of ice into a liquid will increase the overall thickness of the cylindrical D<sub>2</sub> layer from 170 μm to 172 μm because of the lower density of the liquid. This effect in a spherical geometry will be more damaging as the difference in the radius of the outer and inner surfaces of the ice layer will cause the inner surface to buckle as well as expand, and the added roughness will affect the hydrodynamic stability of the implosion.

	Heat load (W)	Heat Flux ( $\text{W}/\text{m}^2$ )	Time exposed to the elements (s)
OMEGA	0.0006	260	0.1
NIF (no reflective coating)	0.023	670	5
NIF (gold reflective coating)	0.0003	9	5
Fusion Energy	0.3 – 1	7,000 – 25,000	0.05
This experiment	0.00045	42	15

Fig. 10. Comparison of heat load and heat fluxes experienced by the  $\text{D}_2$  ice when the protective shrouds are removed and the target is exposed to ambient radiation. These values are compared with the values generated in this experiment.

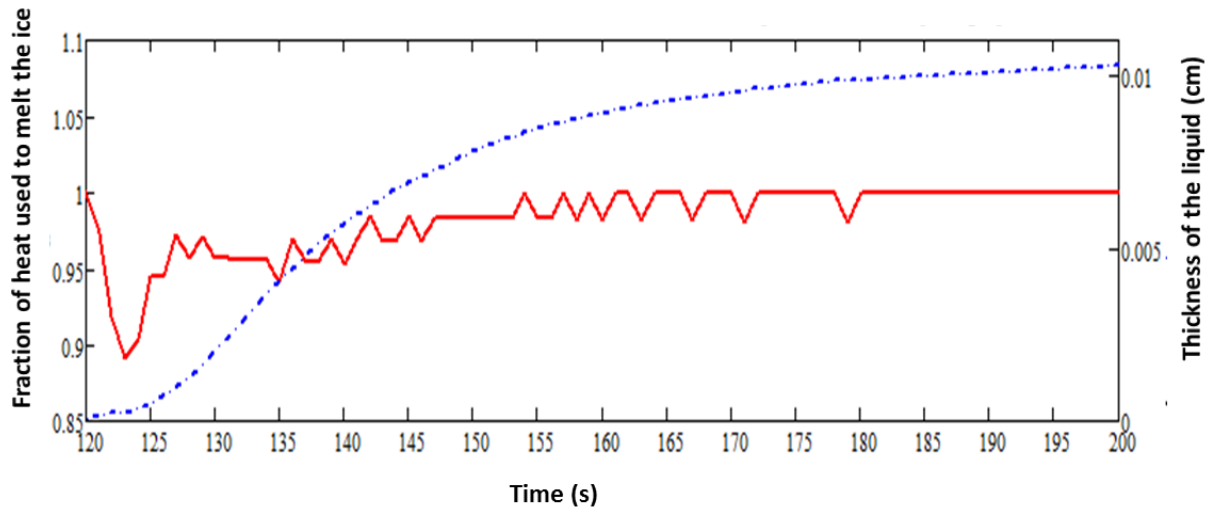


Fig. 11. The fraction of the instantaneous heat (solid red line) used to melt the ice in the experiments of figs. 8 and 9 and the corresponding equivalent thickness of the liquid layer (dotted blue line).

#### **4. Conclusion**

A cryogenic calorimetry cell was used to determine how rapidly a D<sub>2</sub> ice layer melts when a heat load that approximates the radiative load to a NIF target is applied to the cell. Extrapolating these results to a NIF target, it is estimated that a liquid layer, ~4- $\mu$ m thick, will form every second during the first 5 seconds of the target's exposure, and that 90 to 95% of the heat load will be used to melt the ice rather than heat the liquid or sublime the ice.

Two ways to reduce this heating effect are: (i) to decrease the length of time the target is exposed to ambient radiation, or (ii) to maintain the target at a lower initial temperature in the target chamber so that the DT ice does not melt when it warms up. The former approach will require a higher-speed shroud retraction mechanism at the NIF than is currently available, which will complicate the design of the cryogenic equipment. The second approach has more fundamental limitations as cooling the ice well below the triple point temperature compromises the quality of the ice layer, which doesn't recover when the ice subsequently warms.

#### **Acknowledgements**

I'd like to thank Dr. David Harding for guiding me through this project and making sure I not only understood what I was doing but also why it was important; Dr. R. Stephen Craxton for making this research opportunity possible; Kyle Areal-Raines for teaching me how to perform experiments with the calorimetry cell; and Eugene Kowaluk for shooting excellent photos of the calorimetry cell.

## References

1. Harding, D., HAPL Meeting Atlanta GA, Feb 2004  
<http://aries.ucsd.edu/HAPL/MEETINGS/0402-HAPL>
2. Bobeica, M. et. al., Fusion Engineering 2005, Twenty-First IEEE/NPS Symposium.
3. “ Heterogeneous crystal-growth seeds on interior surfaces of ICF capsule” Bernat, T.; Harding, D.; Contract # DE-NA0001369 November 1, 2013